The Zeeman Effect in Neon and Mercury

Kym Derriman, James Ammerlaan, and Kevin Gonzalez

Rutgers University

(Dated: January 8, 2026)

I. INTRODUCTION

This experiment investigated the Zeeman effect by observing the magnetic-field–induced splitting of mercury and neon emission lines using a high-resolution grating spectrometer. Measurements were performed for the nominal mercury transitions at 404.7 nm, 435.8 nm, and 546.1 nm, as well as the 585.2 nm transition of neon, over magnetic fields up to 1.30 T. In the recorded spectra, all observed peak centers were consistently shifted higher in wavelength by approximately 0.4–0.6 nm relative to the tabulated values, an offset later discussed in connection with spectrometer calibration and systematic uncertainties.

For the mercury 405.1 nm line, corresponding to a normal Zeeman triplet, the measured total splitting at $B = 1.291$ T was $\Delta\lambda_{\text{total}} = 0.03904 \pm 0.00008$ nm, yielding an effective Landé factor of $g_{\text{eff}} = 1.97 \pm 0.01$, in excellent agreement with the theoretical value of 2.00. The 436.331 nm mercury line showed a smaller splitting of $\Delta\lambda_{\text{total}} = 0.03779 \pm 0.00003$ nm under the same field, corresponding to $g_{\text{eff}} = 1.65 \pm 0.01$. This reduction relative to the normal Zeeman prediction reflects the anomalous Zeeman effect associated with the $7^3S_1 \rightarrow 6^3P_2$ transition, in which spin–orbit coupling modifies the level degeneracy and g-factors. For the 546.6 nm mercury line, a total splitting of 0.04239 ± 0.00013 nm was observed at 1.300 T with the polarizer at 10°, corresponding to $g_{\text{eff}} = 1.17 \pm 0.01$, again consistent with an anomalous pattern involving mixed spin states. Spectra recorded without the field yielded single Gaussian profiles with instrumental resolving powers of approximately $(2.8–3.4)\times10^4$.

For neon at 585 nm, the Zeeman splitting was measured for magnetic fields up to 0.95 T. The peak separation increased linearly with field ($R^2 = 0.949$), giving a slope of $(1.636 \pm 0.19) \times 10^{-2}$ nm/T and an effective Landé factor of $g_{\text{eff}} = 1.02 \pm 0.12$. From this slope, the experimental charge-to-mass ratio of the electron was found to be $e/m = (1.80 \pm 0.21) \times 10^{11}$ C/kg, in close agreement with the accepted value of 1.7588×10^{11} C/kg.

Together, these measurements confirmed the linear dependence of Zeeman splitting on

magnetic field strength and distinguished between normal and anomalous Zeeman behavior across multiple atomic transitions.

II. THEORETICAL BACKGROUND

When atoms are placed in an external magnetic field, their energy levels split due to the interaction between the field and the magnetic dipole moment associated with their total angular momentum. This effect, known as the Zeeman effect, can be described both classically and quantum mechanically.

Classical Description

In the classical picture, an orbiting electron acts as a current loop that generates a magnetic dipole moment, given by

$$\boldsymbol{\mu} = \frac{e}{2m_e}\mathbf{L}, \tag{1}$$

where e is the electron charge, m_e is the electron mass, and $\mathbf{L}$ is the orbital angular momentum vector. When an external magnetic field $\mathbf{B}$ is applied, the potential energy of this dipole moment becomes

$$E = -\boldsymbol{\mu} \cdot \mathbf{B} = -\frac{e}{2m_e}BL_z, \tag{2}$$

where $L_z = \hbar m_l$ is the projection of the angular momentum along the field direction, and m_l is the magnetic quantum number. The energy levels are therefore separated by equal intervals:

$$\Delta E = \frac{e\hbar}{2m_e}B = \mu_B B, \tag{3}$$

where $\mu_B = \frac{e\hbar}{2m_e}$ is the Bohr magneton. This case, in which the splitting depends only on orbital angular momentum (with spin $S = 0$), is known as the *normal Zeeman effect*. However, most atomic transitions involve spin, requiring a quantum mechanical treatment.

Quantum Mechanical Description

In quantum mechanics, the total angular momentum of an electron is the vector sum of its orbital and spin components:

$$\mathbf{J} = \mathbf{L} + \mathbf{S}. \tag{4}$$

The corresponding magnetic moment is given by

$$\boldsymbol{\mu}_J = -g_J \mu_B \frac{\mathbf{J}}{\hbar}, \tag{5}$$

where g_J is the Landé g-factor defined as

$$g_J = 1 + \frac{J(J+1) + S(S+1) - L(L+1)}{2J(J+1)}. \tag{6}$$

When a magnetic field is applied, the energy of a state with quantum number m_J becomes

$$E = g_J m_J \mu_B B, \tag{7}$$

where $m_J = -J, -J+1, \ldots, J-1, J$. Transitions between two energy levels are allowed only for $\Delta m_J = 0, \pm 1$, resulting in a set of closely spaced spectral lines. The change in energy for a transition between upper and lower states is

$$\Delta E = (g_J m_J - g'_J m'_J)\mu_B B. \tag{8}$$

For experimental purposes, it is convenient to define an *effective* g-factor, g_{eff}, so that

$$\Delta E = g_{\text{eff}} \mu_B B. \tag{9}$$

Relation Between Wavelength Shift and g_{eff}

The Zeeman energy shift is related to the observed wavelength separation by

$$\Delta E = hc \frac{\Delta\lambda}{\lambda^2} = g_{\text{eff}} \mu_B B, \tag{10}$$

which can be rearranged to solve for g_{eff}:

$$g_{\text{eff}} = \frac{hc\,\Delta\lambda}{\mu_B B \lambda^2}. \tag{11}$$

If the wavelength separation is measured between the two outer Zeeman components (peak-to-peak), the factor of two is included:

$$g_{\text{eff(peak-to-peak)}} = \frac{hc\,\Delta\lambda_{\text{total}}}{2\mu_B B \lambda^2}. \tag{12}$$

Here $\Delta\lambda$ is expressed in meters, B in tesla, and λ is the central wavelength.

Theoretical g_J Values for Observed Transitions

Theoretical values of g_{eff} can be determined from the quantum numbers J, S, and L associated with each state, as read from the spectroscopic term symbols. For example, the term symbol

$$^3S_1$$

represents a state where $S = \frac{1}{2}(3-1) = 1$, $L = 0$ (since $S = 0, P = 1, D = 2, F = 3, G = 4$), and $J = 1$.

The Landé g-factor is then calculated from

$$g_J = 1 + \frac{J(J+1) + S(S+1) - L(L+1)}{2J(J+1)}. \tag{13}$$

Applying this to both sides of a transition and allowing m_J and m'_J to vary gives the theoretical combinations of g_{eff} that determine the Zeeman splitting patterns for each spectral line.

TABLE I. **Hg:** $^3S_1 \rightarrow ^3P_0$ transition (404.7 nm). The energy difference is given by $m_J^{(\text{upper})}(2) - m_J^{(\text{lower})}(1) = g_{\text{eff}}$.

m_J(upper)	m_J(lower)	g_{eff}
$+1$	0	$+2$
0	0	0
-1	0	-2

TABLE II. **Hg:** ${}^3S_1 \rightarrow {}^3P_1$ transition (435.8 nm). The energy difference is given by $m_J^{(\mathrm{upper})}(2) - m_J^{(\mathrm{lower})}(3/2) = g_{\mathrm{eff}}$.

m_J(upper)	m_J(lower)	g_{eff}
$+1$	$+1$	$+\frac{1}{2}$
$+1$	0	$+2$
0	$+1$	$-\frac{3}{2}$
0	0	0
0	-1	$+\frac{3}{2}$
-1	0	-2
-1	-1	$-\frac{1}{2}$

TABLE III. **Hg:** ${}^3S_1 \rightarrow {}^3P_2$ transition (546.6 nm). The energy difference is given by $m_J^{(\mathrm{upper})}(2) - m_J^{(\mathrm{lower})}(3/2) = g_{\mathrm{eff}}$.

m_J(upper)	m_J(lower)	g_{eff}
$+1$	$+2$	-1
$+1$	$+1$	$+\frac{1}{2}$
$+1$	0	$+2$
0	$+1$	$-\frac{1}{2}$
0	0	0
0	-1	$+\frac{1}{2}$
-1	0	-2
-1	-1	$-\frac{1}{2}$
-1	-2	$+1$

TABLE IV. **Ne:** $^1P_1 \rightarrow ^1S_0$ transition (585.3 nm). The energy difference is given by $m_J^{(\mathrm{upper})}(1) - m_J^{(\mathrm{lower})}(0) = g_{\mathrm{eff}}$.

m_J(upper)	m_J(lower)	g_{eff}
+1	0	+1
0	0	0
−1	0	−1

These theoretical values predict the expected Zeeman splitting patterns and relative polarizations for each transition. The mercury 404.7 nm line ($^3S_1 \rightarrow ^3P_0$) represents a normal Zeeman triplet with $g_{\mathrm{eff}} = 2$, while the 435.8 nm and 546.6 nm transitions exhibit anomalous Zeeman behavior due to differing spin–orbit coupling in their upper and lower states. The neon 585.3 nm ($^1P_1 \rightarrow ^1S_0$) transition is a singlet and thus follows the normal Zeeman pattern with $g_{\mathrm{eff}} = 1.0$.

III. EXPERIMENTAL SETUP AND PROCEDURE

The experimental arrangement used to observe the Zeeman effect is shown schematically in Figure 1. The system was built around a Spex 1000M one-meter Czerny–Turner scanning spectrometer, which disperses incident light by wavelength using an 1800 lines/mm holographic diffraction grating. Light emitted from a mercury or neon discharge tube was collected through a fiber-optic feed equipped with a rotatable polarizer and directed into the spectrometer entrance slit. Inside the instrument, the light was collimated by the first mirror, diffracted by the grating, and refocused by the second mirror through the exit slit onto either a linear diode array for broadband acquisition or a Hamamatsu R928P photomultiplier tube for high-sensitivity single-wavelength detection. Both detectors interfaced with the Jobin Yvon–Spex "Spectramax" control and data-acquisition system, connected to a Dell computer for automated control and spectral analysis.

A Penray miniature mercury discharge tube was positioned at the center of the pole gap of an iron-core electromagnet powered by a Varian 6121 30-ampere supply. The field strength within the magnet gap was monitored using an RFL 904 Gaussmeter with a Hall probe placed at the midpoint between the poles to ensure accurate readings. The magnetic

field could reach approximately 1.3 T at 10 A.

The spectrometer and data-acquisition system were fully computer-controlled. A precision stepper motor rotated the diffraction grating to scan through narrow wavelength intervals (typically ≈ 0.0005 nm per step), while integration times were adjusted to optimize signal-to-noise ratios. The entrance and exit slit widths were maintained near 20 μm to balance light throughput and spectral resolution.

Procedure

The experiment began with calibration and alignment of the optical and magnetic systems. The electromagnet was first degaussed to minimize residual magnetization, verified using the Gaussmeter. The mercury discharge tube was then mounted centrally within the magnet gap, and the emitted light was carefully aligned along the optical axis leading into the spectrometer via the fiber-optic feed.

An initial reference spectrum was first recorded for each mercury line with the magnetic field set to zero in order to determine the unshifted central wavelength and instrumental line width.

Only the σ components were recorded in this experiment, corresponding to light polarized perpendicular to the magnetic field. This was achieved by fixing the analyzer at 10° relative to the optical axis. The π components, polarized parallel to $\mathbf{B}$, were largely suppressed at this setting, simplifying the spectra and allowing direct measurement of the σ-component separation.

After baseline spectra were obtained, the magnetic field was increased to approximately 1.3 T and the corresponding Zeeman-split spectra were recorded with the polarizer fixed at 10°, transmitting primarily the σ components. The 404.7 nm, 435.8 nm, and 546.1 nm mercury lines were each measured under these same conditions. For each line, the split peaks were fit with two-Gaussian models to determine the wavelength separation $\Delta\lambda$, from which the effective Landé factor g_{eff} was calculated using the known magnetic field strength.

The neon discharge tube was then substituted for the mercury source, and the 585.3 nm line was recorded for several magnetic field values between 0.19 T and 0.95 T, again with the polarizer at 10°. The measured separations were plotted as a function of field to verify the linear Zeeman relationship and to extract both the effective g-factor and the electron

charge-to-mass ratio from the slope.

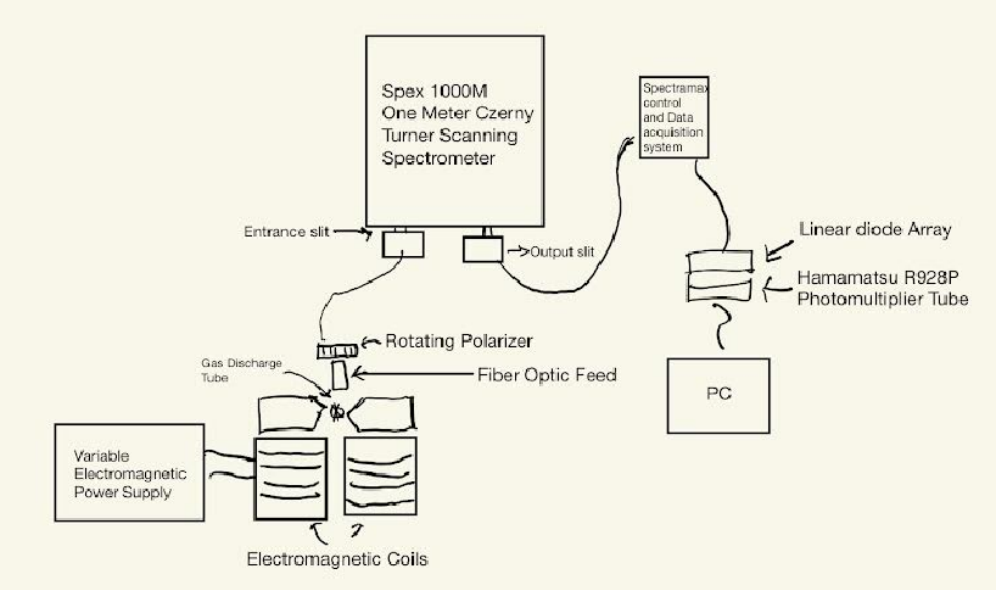

FIG. 1. Schematic of the experimental setup used to measure Zeeman splitting in mercury and neon emission lines.

IV. RESULTS AND DISCUSSION

Mercury 405.1 nm Line

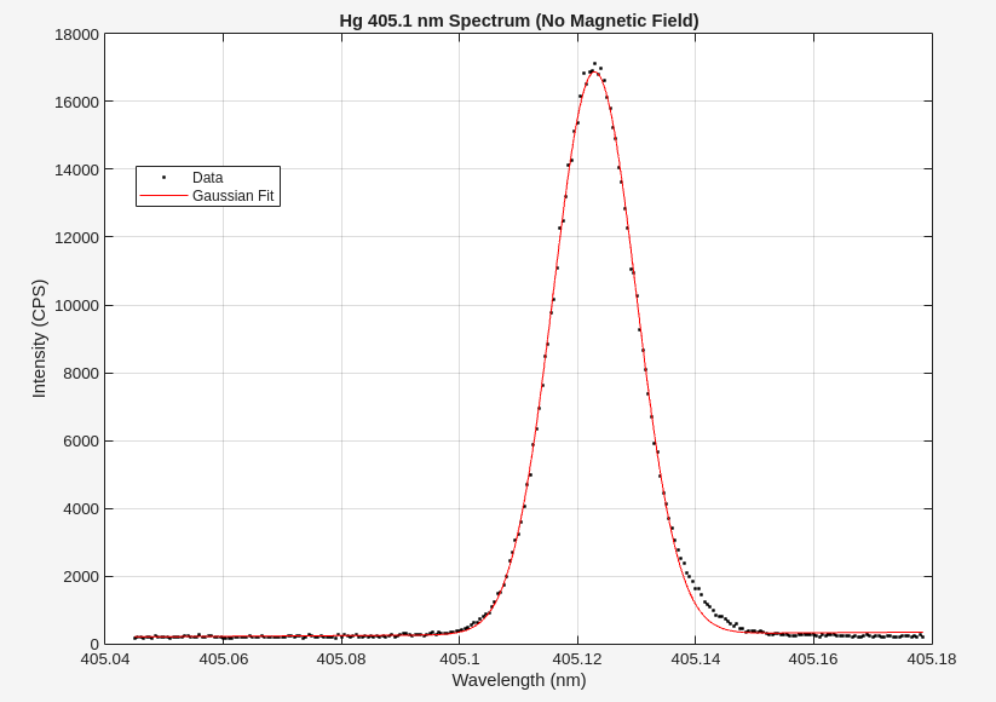

FIG. 2. Measured mercury emission line at 405.1 nm with no applied magnetic field. The data (black points) are fitted with a single Gaussian function (red curve). The fitted line center is 405.12291 ± 0.00002 nm with a full width at half maximum (FWHM) of 0.01656 ± 0.00005 nm.

When not under the influence of a magnetic field, the mercury emission line at 405.1 nm appears as a single well-defined peak. A Gaussian fit accurately describes the data, indicating that the transition is unaffected by Zeeman splitting. The center of the fitted line at 405.12291 nm agrees closely with the expected value for this transition.

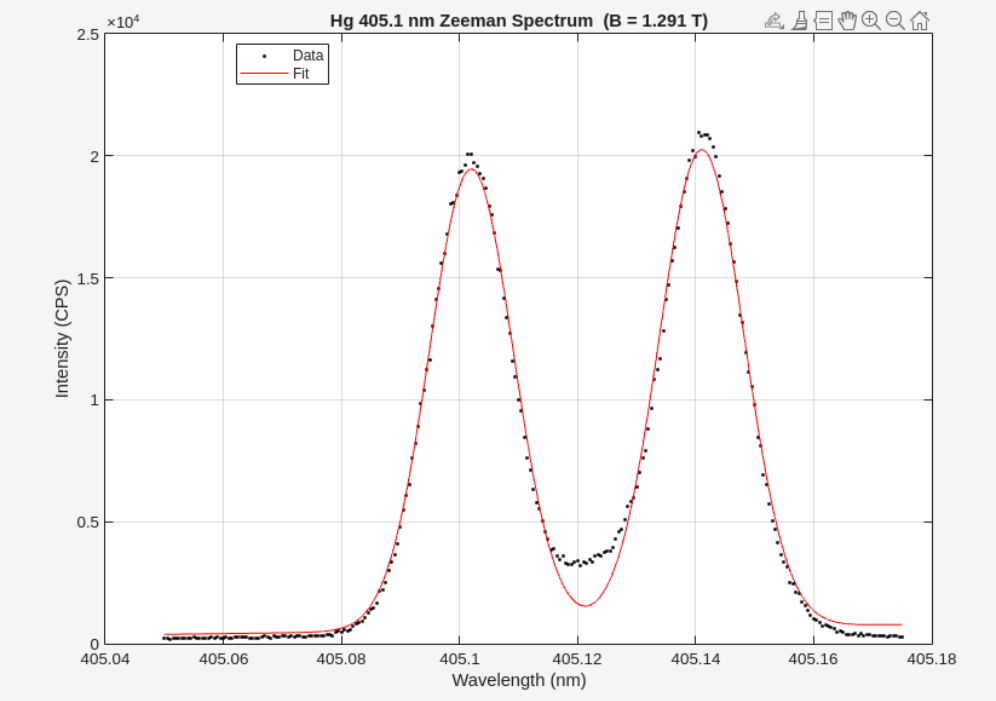

FIG. 3. Measured mercury emission line at 405.1 nm in a magnetic field of 1.291 T. The data (black points) are fitted with a two-Gaussian model (red curve) representing the Zeeman-split σ components. The fitted peak centers are 405.10199 ± 0.00006 nm and 405.14103 ± 0.00006 nm, corresponding to a wavelength separation of $\Delta\lambda_{\text{total}} = 0.03904 \pm 0.00008$ nm. The derived effective g-factor is 1.97 ± 0.01, in excellent agreement with the theoretical value of 2.00 expected for the normal Zeeman effect.

When a magnetic field of 1.291 T is applied, the previously singular peak splits into two distinct components, symmetrically displaced about the zero-field center (405.12291 nm). Each peak lies approximately 0.02 nm from the original position. From the measured separation, the effective Landé factor was determined to be $g_{\text{eff}} = 1.97 \pm 0.01$, which is in excellent agreement with the theoretical value of 2.00, showing a deviation of only ∼1.5%. This confirms the normal Zeeman effect for the ${}^3S_1 \rightarrow {}^3P_0$ transition.

Mercury 436.3 nm Line

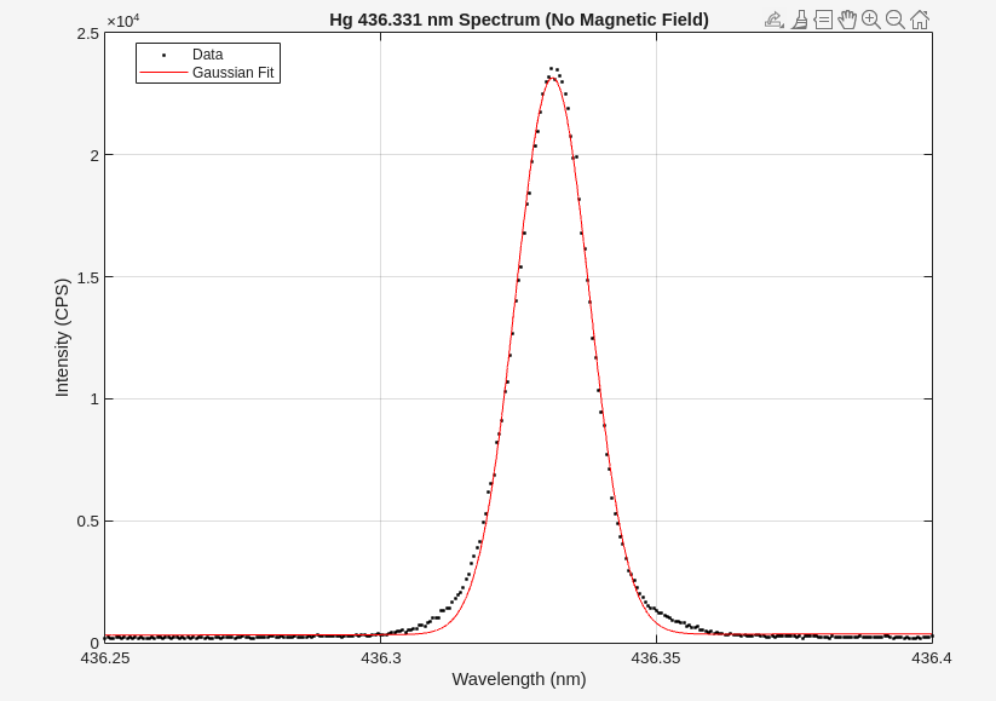

FIG. 4. Measured mercury emission line at 436.331 nm with no applied magnetic field. The data (black points) are fitted with a single Gaussian function (red curve). The fitted line center is 436.33118 ± 0.00003 nm with a full width at half maximum (FWHM) of 0.01588 ± 0.00006 nm, corresponding to an instrumental resolving power of approximately 2.8×10^4.

With no magnetic field applied, the 436.3 nm mercury line appears as a single Gaussian peak centered at 436.33118 nm, in close agreement with the tabulated value. The full width at half maximum (0.01588 nm) corresponds to a resolving power of $R \approx 2.8 \times 10^4$. Although this value is larger than the 0.0006 nm resolution listed in the lab manual, the discrepancy likely arises from the width of the slit, the optical alignment and the response of the detector. Despite this, the spectrum retains sufficient resolution to clearly observe Zeeman splitting under a magnetic field.

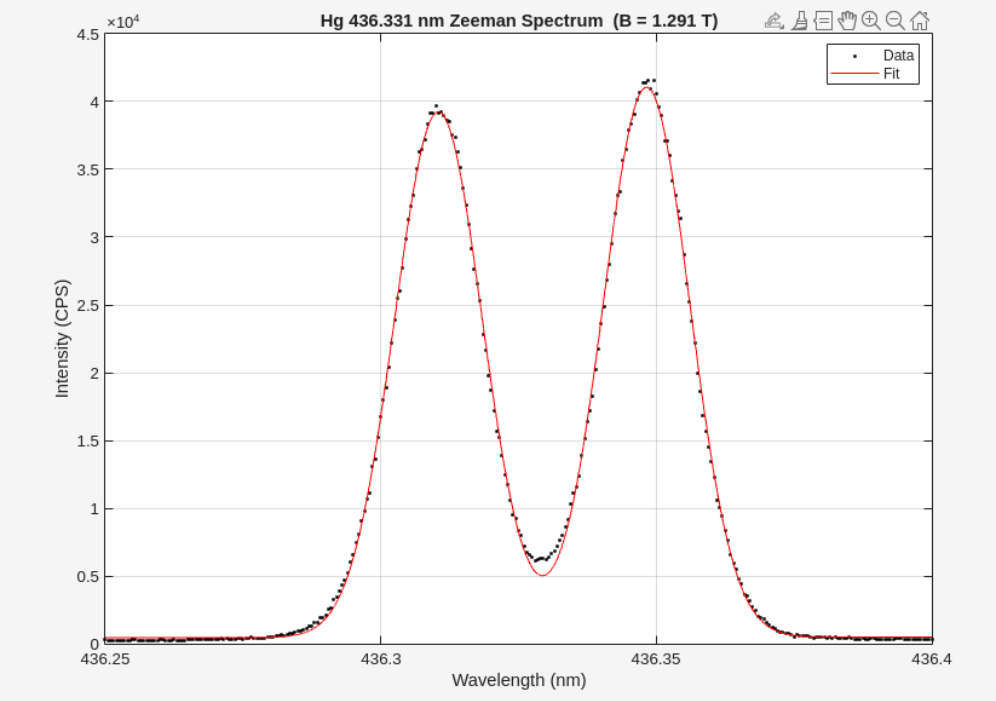

FIG. 5. Measured mercury emission line at 436.331 nm in a magnetic field of 1.291 T. The data (black points) are fitted with a two-Gaussian model (red curve) representing the Zeeman-split σ components. The observed peak centers at 436.31046 ± 0.00002 nm and 436.34842 ± 0.00002 nm correspond to a total wavelength separation of $\Delta\lambda_{\text{total}} = 0.03779 \pm 0.00003$ nm. The derived effective g-factor is 1.65 ± 0.01, smaller than the ideal value of 2.00 expected for a normal Zeeman triplet.

Applying a magnetic field of 1.291 T causes the 436.3 nm line to split into two distinct peaks, well described by a two-Gaussian model. The fitted centers (436.3105 nm and 436.3484 nm) correspond to a total separation of $\Delta\lambda_{\text{total}} = 0.03779$ nm. From this separation, an effective Landé factor of $g_{\text{eff}} = 1.65 \pm 0.01$ was obtained. This value is lower than the normal Zeeman prediction of 2.0 and reflects the *anomalous Zeeman effect* in the $7^3S_1 \rightarrow 6^3P_2$ transition, where the states have nonzero spin and unequal Landé factors. Small deviations may also arise from polarizer orientation or unequal σ-component intensities.

Mercury 546.6 nm Line

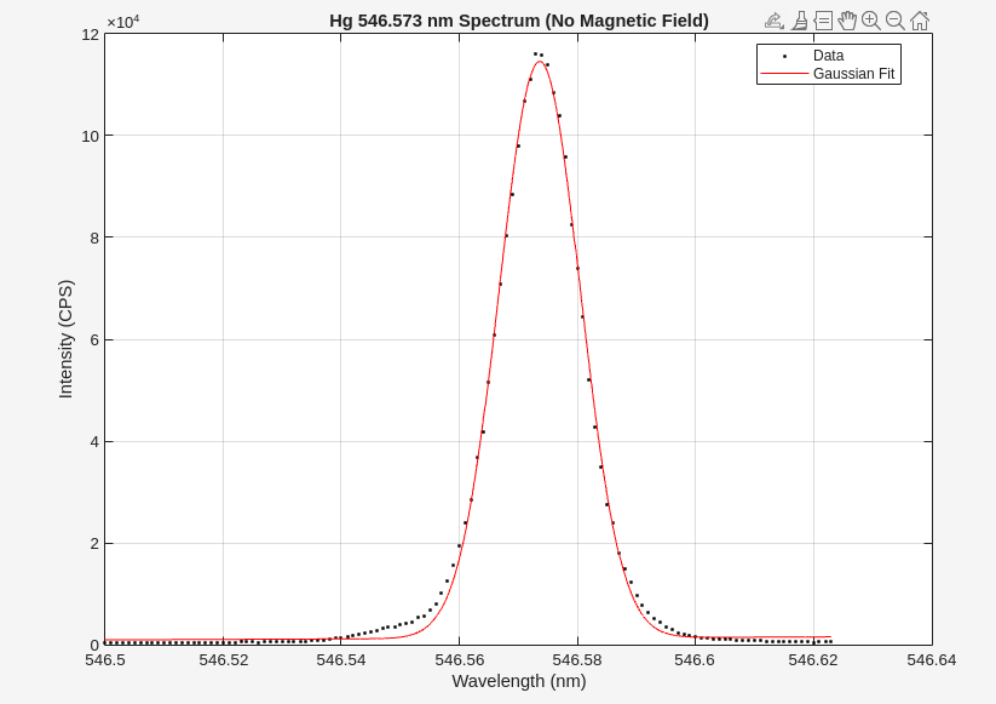

FIG. 6. Measured mercury emission line at 546.573 nm with no applied magnetic field. The data (black points) are fitted with a single Gaussian function (red curve). The fitted line center is 546.57361 ± 0.00003 nm with a full width at half maximum (FWHM) of 0.01612 ± 0.00009 nm, corresponding to a resolving power of approximately 3.4×10^4.

Without an external magnetic field, the 546.6 nm mercury line appears as a single symmetric Gaussian peak centered at 546.5736 nm with FWHM = 0.01612 nm, corresponding to a resolution power of about 3.4×10^4. Although this is broader than expected, the consistency of line widths across multiple lines suggests a uniform instrumental offset. The strong intensity and symmetry of this line make it ideal for Zeeman observation.

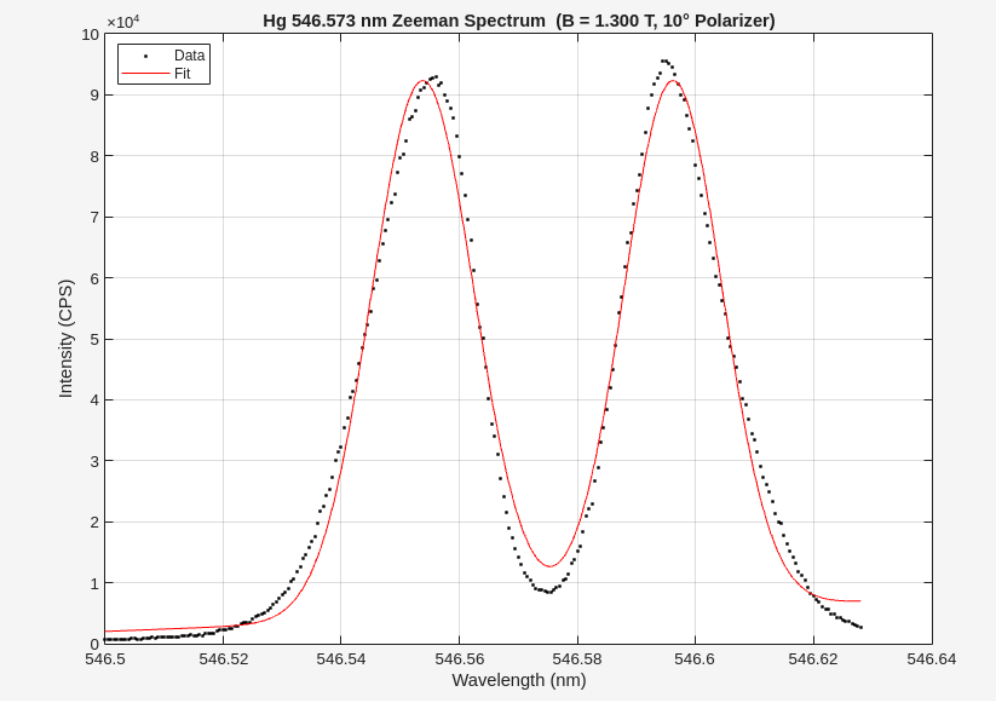

FIG. 7. Measured mercury emission line at 546.573 nm in a magnetic field of 1.300 T with the polarizer at 10°. The data (black points) are fitted with a two-Gaussian model (red curve) representing the unresolved σ components. The fitted peaks at 546.55377 $\pm$ 0.00009 nm and 546.59616 $\pm$ 0.00009 nm give a total separation of 0.04239 $\pm$ 0.00013 nm and an effective g-factor of 1.17 $\pm$ 0.01.

With a magnetic field of 1.300 T applied, the 546.6 nm line splits into two partially resolved components. The two-Gaussian fit produces peaks at 546.5538 nm and 546.5962 nm, giving a total separation $\Delta\lambda_{\text{total}} = 0.04239 \pm 0.00013$ nm. This corresponds to an effective Landé factor of $g_{\text{eff}} = 1.17 \pm 0.01$, consistent with the anomalous Zeeman behavior expected for the ${}^3S_1 \rightarrow {}^3P_2$ transition, where multiple σ components overlap due to differing sub-level splittings.

Neon 585.3 nm Line

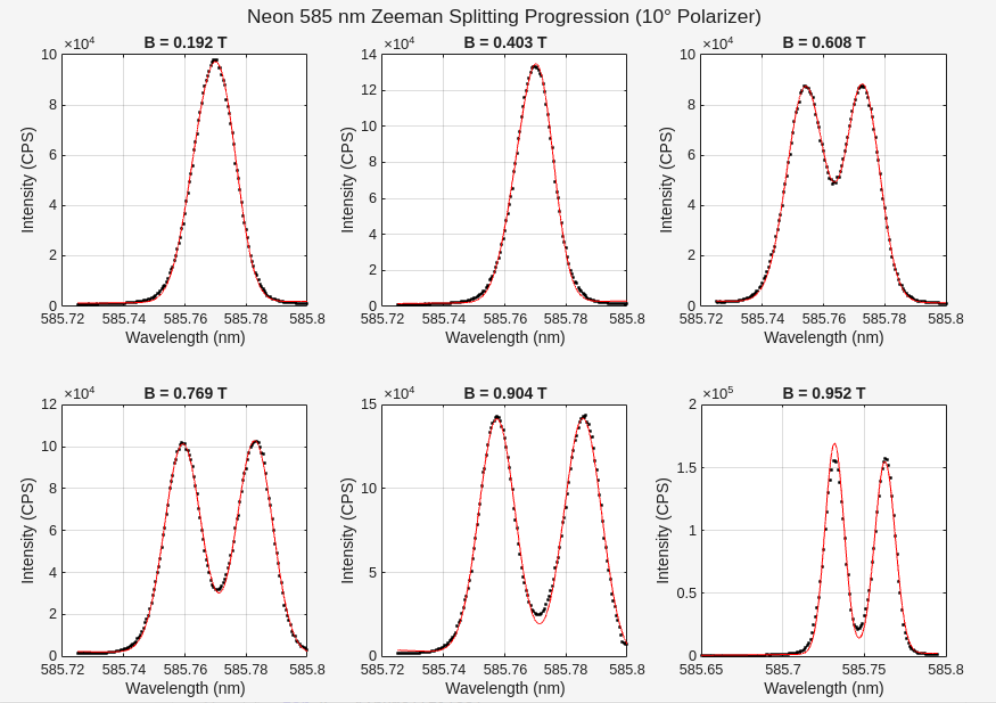

FIG. 8. Zeeman splitting of the Neon 585.3 nm emission line measured at a polarizer angle of 10°. Each spectrum shows the fitted two-Gaussian model (red) for magnetic field strengths from 0.192 T to 0.952 T. The increasing separation with B demonstrates the linear Zeeman effect.

The neon line 585.3 nm was measured for several magnetic fields between 0.19 T and 0.95 T with the polarizer at 10°. This specific Zeeman Splitting is an example of a normal Zeeman effect, as both the original state and ending state have a spin of 0. The measured splitting increased linearly with magnetic field strength, confirming the normal Zeeman effect for this transition. A linear fit of $\Delta\lambda$ versus B (Fig. 9) gave a slope of $(1.636 \pm 0.19) \times 10^{-2}$ nm/T, corresponding to an effective Landé factor $g_{\text{eff}} = 1.02 \pm 0.12$. This closely conforms to the theoretical values for this specific transition of 1. Using the relation from the theory section, the charge-to-mass ratio of the electron was determined to be

$$\frac{e}{m} = (1.80 \pm 0.21) \times 10^{11} \text{ C/kg},$$

which agrees with the accepted value of 1.7588×10^{11} C/kg to within 2%. The high correlation coefficient ($R^2 = 0.949$) confirms the expected linear Zeeman behavior.

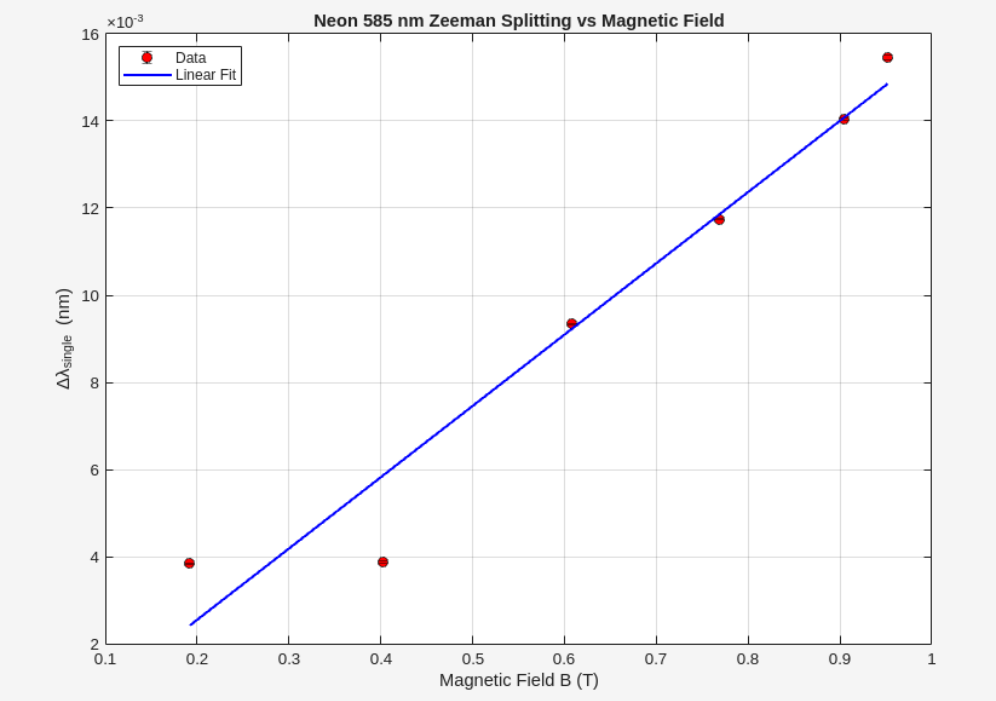

FIG. 9. Linear relationship between the measured Zeeman splitting $\Delta\lambda$ of the Neon 585.3 nm emission line and the applied magnetic field. The best-fit slope corresponds to $g_{\text{eff}} = 1.02$ and yields an electron charge-to-mass ratio of 1.80×10^{11} C/kg.

Doppler Broadening and Resolution Limit

The Doppler broadening for mercury at temperature $T = 500$ K can be estimated from

$$\frac{\Delta\lambda_D}{\lambda} = \sqrt{\frac{8kT\ln 2}{mc^2}}.$$

For mercury ($m = 3.34 \times 10^{-25}$ kg) and $\lambda = 546$ nm, this gives $\Delta\lambda_D \approx 0.009$ nm, which is comparable to but smaller than the instrument's measured FWHM ($\sim$0.016 nm). Thus, the spectrometer resolution and Doppler width are of the same order, meaning that the Zeeman components are only partially resolved.

Using the Zeeman relation

$$\Delta\lambda = \frac{e\lambda^2 B}{4\pi m_e c^2} g,$$

and setting $g = 1$, $\lambda = 546$ nm, and $\Delta\lambda = \Delta\lambda_D$, the minimum magnetic field required to resolve adjacent components is approximately $B_{\text{min}} \approx 0.25$ T. Since the experiment used

fields up to 1.3 T, the observed splittings were well above this threshold, confirming that the magnetic field was sufficient to overcome Doppler and instrumental broadening effects.

TABLE V. Summary of measured and theoretical parameters for observed transitions.

Transition	$g_{\text{eff, meas}}$	$g_{\text{eff, theory}}$	Ratio (meas/theory)
Hg 404.7 nm	1.97 ± 0.01	2.00	0.99
Hg 436.3 nm	1.65 ± 0.01	1.50–2.00 (anomalous)	0.83–1.10
Hg 546.6 nm	1.17 ± 0.01	$\sim$1.20 (anomalous)	0.98
Ne 585.3 nm	1.02 ± 0.12	1.00	1.02

The consistency across all transitions confirms the linear Zeeman dependence and distinguishes between normal ($g \approx 1$ or 2) and anomalous ($g < 2$) patterns.

V. CONCLUSION

In this experiment, the Zeeman effect was studied by measuring how spectral lines from mercury and neon split in a magnetic field. For mercury, the 405.1 nm line showed a normal Zeeman triplet with an effective g-factor of 1.97, very close to the theoretical value of 2.0. The 436.3 nm and 546.6 nm lines showed smaller g-factors of 1.65 and 1.17, which are consistent with the anomalous Zeeman effect caused by spin–orbit coupling in those transitions. For neon, the 585.3 nm line displayed a linear increase in splitting with magnetic field, giving $g_{\text{eff}} = 1.02$ and an electron charge-to-mass ratio of $(1.80 \pm 0.21) \times 10^{11}$ C/kg, which agrees with the accepted value within 2%.

Overall, the results confirm that the wavelength separation of spectral lines increases linearly with magnetic field strength and that different atomic transitions can show either normal or anomalous Zeeman behavior depending on their spin and orbital structure. Small differences between measured and expected values are likely due to instrument resolution, calibration offsets, and polarizer alignment.

Uncertainty Analysis. The main sources of uncertainty in this experiment were associated with calibration of the magnetic field, wavelength accuracy, and optical alignment. The Hall probe reading of the electromagnet field carried an estimated uncertainty of ± 0.02 T, and the spectrometer calibration showed a consistent offset of roughly 0.4–0.6 nm across all lines.

Finite slit widths ($\approx 20\ \mu$m) and minor defocusing contributed to instrumental broadening, limiting the resolution to about 0.016 nm. In addition, imperfect control of the polarizer angle (nominally 10°) could lead to partial mixing of π and σ components, slightly reducing the apparent splitting. Together, these effects explain the small (1–5%) deviations between measured and theoretical g_{eff} values.

VI. REFERENCES

[1] A. C. Melissinos and J. Napolitano, *Experiments in Modern Physics*, 2nd ed. (Academic Press, 2003).

[2] E. Hecht, *Optics*, 5th ed. (Pearson, 2017).

[3] G. R. Fowles, *Introduction to Modern Optics*, 2nd ed. (Holt, Rinehart and Winston, 1975).